



Three Dimensional Modeling of Pulsed Fusion for Propulsion and Terrestrial Power Using Smooth Particle Fluid with Maxwell Equation Solver (SPFMax)

Jason T. Cassibry¹ Ross Cortez², Coleton Cody³, Seth Thompson, Lloyd Jackson
University of Alabama in Huntsville, Huntsville, AL 35899

This paper presents a 3D plasma model developed from the ground up to support research in magneto-inertial fusion. The physics include shock capturing, tabular equations of state, viscosity, heat transfer, radiation, and fast ion stopping power models. One of the main challenges is to produce a code with a self-consistent circuit model and electromagnetic field solver. The circuit model is approximated as a 3D network of transmission lines connected to the external circuit, and this models current and voltage throughout the domain including both plasma and solid conductors. Vacuum and dielectric field propagation is modeled with the finite difference time domain. The code physics are documented for completeness, but emphasis is placed on the circuit and electromagnetic field models. A preliminary simulation of a magnetized target compressed by a surrounding Argon liner is performed, showing a 100 fold increase in density and temperature increase from 80 to 1000 eV in the target. The simulation crashed at 600 ns, but showed steady increase in fusion energy and neutron yield. The magnetic field topology evolved over time, but remained a closed field line configuration through the simulation, maintaining roughly 1 T in the target.

I. Introduction

The abundance of deuterium, lithium, boron, and hydrogen on Earth combined with the energy storage density of $\sim 10^{14}$ J/kg available makes controlled thermonuclear fusion an attractive candidate for terrestrial power production[1] and advanced propulsion[2]. Fusion has been pursued in this manner for over 60 years and the only systems that have released more fusion product energy than invested in the system are thermonuclear bombs and stars, neither of which make convenient reactors.

There are two problems that make fusion very challenging. A number of textbooks discuss this matter in more detail (see Refs. [3], [4] for example). First, the charged particle reactants have to overcome long range repulsive Coulomb forces which dominate over the attractive strong force for distances greater than a few femtometers, and this scale size is only as ‘big’ as it is because of the benefits of quantum tunneling. In a thermal plasma, the cross this requires temperatures of ~ 10 keV (10^8 K). The high temperature poses additional challenges which are consequences of overcoming the Coulomb barrier, including efficient drivers for heating plasmas to these temperatures, containment of high temperature plasmas, and significant radiation losses which

¹ Associate Professor, Propulsion Research Center, Lifetime Associate Member.

² Research Engineer, Aerophysics Research Center, Student Member

³ Undergraduate Research Assistant, Propulsion Research Center

can easily outpace the fusion energy production. The second challenge requires a bit more explanation. Reaching the temperatures needed requires a specific internal energy of 10^{12} J/kg, and when driver inefficiencies and incomplete fuel burnup are factored in, this can escalate to an effective energy invested exceeding the total energy released by the fusion reactions. Inertial fusion concepts rely on heating only a small fraction of the fuel mass, a so-called hotspot in the center of a dense fuel layer, and the charged products generated from the hotspot are intended to deposit energy locally to burn a surrounding cold fuel layer. Therein lies the second challenge, because the charged products are ‘born’ moving at about 10^7 m/s requiring a number of collisions prior to thermalizing. For a sense of scale, a plasma at air density of 10^{25} #/m³ would require a meter of plasma to stop a single ion. As an analogy, one could imagine the inconvenience of using a lighter if the sparks from the flint had to heat a 1 m³ volume of gas in order to achieve ignition of a flame! To stop the fusion products locally, liquid density ($\sim 10^{28}$ #/m³) or higher fuels or high magnetic fields (100’s of Tesla) are required. A strong magnetic field can trap the charged products as long as the Larmor radius(see for example [5]) is smaller than the fuel volume. For example, a 400 T field gives a Helium ion with velocity of 10^7 m/s a Larmor radius of 1 mm.

The nascent field of magneto-inertial fusion (MIF) [1] is a confinement approach in which a spheroidal or cylindrical target of plasma is compressed by an imploding liner. A recent popular press article in Scientific American discusses several variants on this topic[6]. Because of the detailed vehicle design study performed by Adams et al[7] using the plasma jets driven magneto-inertial fusion (PJMIF)[8] concept, we will focus on the PJMIF approach. In PJMIF, a spherical array of plasma jets are launched at hypervelocity towards a magnetized target, Fig. 1a. The jets coalesce into a spherical liner which compresses the target, Fig. 1b. MIF has features which make it an attractive confinement approach for fusion propulsion. First, the density regime is between 10^{25} and 10^{29} ions/m³, roughly spanning molecular density of air at sea level to solid density, so the reacting volume is only 1 to 10 cm³, and the total energy prior to fusion burn can potentially be less than 10^6 J[9]. Second, the presence of the magnetic field suppresses cross field electron thermal conduction, reducing the heat loss which is severe since the thermal conductivity scales with the electron temperature as $T_e^{5/2}$. This reduces the power required to compress and heat the target to Gigawatt (GW) to Terawatt (TW) scale pulsed power systems, which are already in existence.

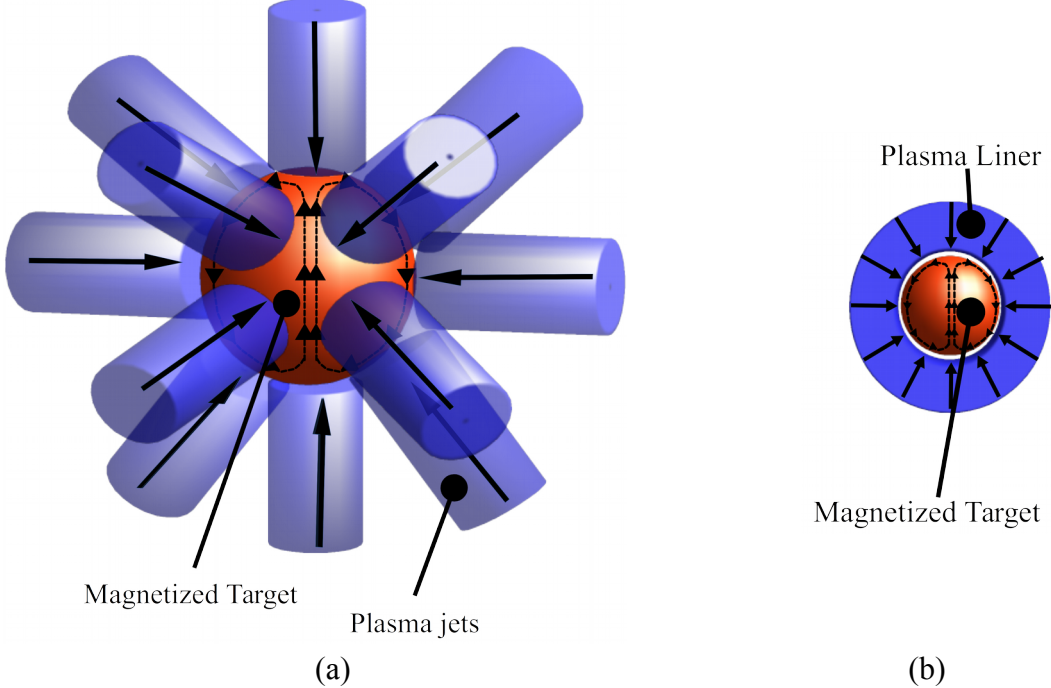


Figure 1. In Plasma jet driven magneto-inertial fusion (PJMIF), (a), a spherical array of plasma jets implodes on a magnetized target, and (b) the jets coalesce into a spherical plasma liner which compresses the target.

A number of plasma codes will be needed to flesh out the physics in support of experiments and are available. The state of the art in multidimensional modeling spherical implosions in the MIF physics regimes include the 3D Rad-Hydro Code HYDRA[10], the MACH family of codes[11], the 2D axisymmetric MHD code LASNEX[12], and state of the art particle-in-cell codes like LSP[13]. HYDRA is an Eulerian code that lacks the ability to couple plasmas to external circuits in a self-consistent manner. LASNEX can model magnetic fields, but only in axisymmetric geometries. MACH3 can model all of these effects, but does not have a model for nonlocal deposition of fusion products. PIC codes like LSP can model all of these effects, but are very demanding on computational resources. Parametric sweeps require a prohibitively large amount of computational power. Finally, it is difficult to model 3D problems with anything short of a highly parallel supercomputer.

We decided to develop a new 3D code to support our research in MIF(see for example Refs. [14]–[16]) with the goal of making it reasonably accurate but with the ability to run on a laptop to facilitate rapid turn around on simulations. The physics required to model a fusion plasma include tabular equations of state to model variable levels of ionization, thermal conduction, radiation emission and absorption, shock capturing, real viscosity, electromagnetic field propagation and forces in the plasma, a self-consistent circuit model, and nonlocal absorption of fusion ion product energy. The code also needs to resolve vacuum/plasma interface and nonlocal transport of charged particle deposition, heat transfer, radiation, shock capturing, and viscosity.

To accomplish this, we have developed from scratch a new multiphysics code which is vectorized and GPU-enabled in Matlab called Smooth Particle Hydrodynamics with Maxwell equation solver (SPFMaX).

Of all the physics listed above, by far the most difficult part to develop has been the electromagnetic equation solver. The reason is because we did not want to use magnetohydrodynamic (MHD) approximation[17] in which the time derivative of electric field is neglected, leading to the application of the magnetic induction equation (i.e. a combination of Ohm's law, Faraday's law, and Ampere's law). The MHD approach has limitations, especially at the vacuum/plasma interface and wherever it is needed to propagate electromagnetic waves across a vacuum or dielectric. Further, numerical solutions to the magnetic induction equation lead to nonzero divergence of magnetic field, although various models have divergence cleanup or divergence free algorithms[18]–[20]. For vacuum wave propagation, the finite difference time domain (FDTD)[21] works well for electromagnetic wave propagation in vacuum and dielectrics and lumped element circuit models, but breaks down when current density dominates Ampere's law. Circuit models are easy to implement, but only couple through boundary conditions and seamless, self-consistent models are difficult. Our approach is to model all conductive paths via a 3D network of transmission lines using Kirchoff's voltage and current laws, with Maxwell's equations solved in the form of the electric scalar and magnetic vector potential.

The rest of the paper is organized as follows. The basic formulation of the smooth particle hydrodynamic method, implementation of the transmission line equations, electric scalar potential and magnetic vector equations, as well as a brief description of the method for nonlocal deposition of radiation is given in section 2. Section 3 gives the initial conditions for the simulation of a plasma liner compressing a magnetized target predicted to give a high gain using 1D LASNEX simulations[22]. Section 4 gives the results for the simulation, followed by conclusions in section 5.

II. SPFMaX Numerical Model

A Smooth Particle Hydrodynamic Method

At the very core of this code is the smooth particle hydrodynamic (SPH) method[23], in which properties are approximated with the integral or kernel approximation according to

$$A_a(r) = \int A(r') W(r - r', h) dr' \quad (1)$$

where A is any property (like temperature, pressure, etc), subscript a means point a , r is the position of point a in space, and W is the interpolating kernel function. In the limit that $h \rightarrow 0$, W becomes the direct delta function and the expression becomes exact. Any function can be approximated in this way, and this is the first assumption of SPH. The second is to replace the integral with a summation,

$$A_a = \sum_b A_b V_b W_{ab}(r - r', h) \quad (2)$$

where V_b is the volume of the neighboring particles b . This is called the summation or particle approximation. This is done because we can't solve the problem at every point in space because computers are finite. The kernel function W is usually a Gaussian-like or cubic b-spline function which goes to zero at some κh , where $\kappa=2$ normally. Gradients can be approximated as

$$\nabla A_a = \sum_b A_b V_b \nabla W_{ab}(r - r', h) \quad (3)$$

In SPFMax, the cubic spline function is used,

$$W_{ab} = \begin{cases} \frac{1}{4\pi h_{ab}^3} [(2-q)^3 - 4(1-q)^3], & \text{for } 0 \leq q \leq 1 \\ \frac{1}{4\pi h_{ab}^3} (2-q)^3, & \text{for } 1 \leq q \leq 2 \\ 0 & \text{for } q > 2 \end{cases} \quad (1)$$

B Finding the compact support distance (h) for each particle

The key to implementing any SPH method properly is to have an accurate list of neighbors for each particle and a compact support distance h which scales the kernel function and its gradients so the following constraints are satisfied

$$\sum_b V_b W_{ab} = 1 \quad (4)$$

and

$$\sum_b V_b \nabla W_{ab} = 0 \quad (5)$$

The particle volume is

$$V_a = \frac{h_a^3}{\eta^3} \quad (6)$$

and η is 1.11. **It cannot be emphasized enough that if Eqs 5 and 6 are not satisfied, the code is not going to produce accurate results at all.** In practice, it is very difficult to choose a compact support distance for each particle to satisfy this everywhere. In SPFMax, h is uniquely found for each particle to satisfy the first constraint, Eq 5, to within 1%, and then the weights W_{ab} and ∇W_{ab} are scaled so that Eqs 5 and 6 are satisfied to within machine accuracy.

For clarity, this procedure is described below. First, particle position is tracked with

$$\frac{\partial r}{\partial t} = u \quad (7)$$

Next, the particle neighbors have to be determined, and SPFMax uses the k-d tree to return the 60 nearest neighbors for each point in a script called `update_neighbors.m`. The commands below are used

```
p.NS = createns(pts);
```

```
[p.nbrs,p.r] = knnsearch(p.NS,pts,'K',60);
```

where 'pts' stores the x,y,z information, and the nbrs and Euclidean distances are stored in 'nbrs' and 'r', respectively. To facilitate vector calculations, each particle has 60 neighbors so the nbrs matrix is a uniform, fixed block of memory. This is done even though the outer 15 or so rarely contribute to the summation interpolant for computational speedup at the expense of memory. Once this has been done, h first is estimated to be half of the maximum distance between the particle and its neighbors. An iterative Newton-Raphson method is then used to improve the h estimate as follows. The particle volume is evaluated at $h+\delta h$ and $h-\delta h$, in which δh is $\sim h/0.01$. After this is done, the cubic spline kernel function is evaluated for $h+\delta h$ and $h-\delta h$. Equation 5 is then used to evaluate the particle consistency at the two values for h , and this is used to find the difference between the two summations. The value for h is then updated with

$$h_a = \frac{2\delta h_a}{\left(\sum_b V W_{ab}\right)_{h_a+\delta h} - \left(\sum_b V W_{ab}\right)_{h_a-\delta h}} \text{sign} \left[1 - \sum_b V_b W_{ab} \right] \min \left(\left| 1 - \sum_b V_b W_{ab} \right|, 0.2 \right) \quad (8)$$

This entire process is then repeated five times. The kernel weights (W_{ab}) are then scaled uniformly for the neighbors to force particle consistency, and this scaling change the value of h by up to $\sim 1\%$. Once h is determined, the particle masses on the first time step should be determined to be consistent with the initial density specified in the input file, and calculation of density is described below. The linear consistency constraint can also be enforced exactly by scaling either all of the negative or positive contributions to the summation of $V_b \nabla W_{ab}$ for each particle over its neighbors. While numerous authors have explored more mathematically rigorous ways of achieving this, we found this to be very robust for our code.

C Equations of motion

SPFMax solves the single fluid equations of motion. Conservation of mass is given by

$$\frac{\partial \rho}{\partial t} + \nabla \cdot (\rho \mathbf{u}) = 0 \quad (9)$$

where ρ (kg/m³) is the mass density, \mathbf{u} is the velocity vector, and t is time. SPFMax solves conservation of mass exactly because the continuity equation is not solved. Rather, density is determined by the particle mass divide by the particle volume, where the mass is a constant property of the particles. SPFMax computes the density from

$$\rho_a = \sum_b m_b W_b \quad (10)$$

The momentum equation for a single fluid is given by

$$\frac{\partial \mathbf{u}}{\partial t} = -\frac{1}{\rho} \nabla p + \nabla \cdot \tau + \frac{1}{\rho} \mathbf{j} \times \mathbf{B} \quad (11)$$

where p is the static pressure and τ is the deviatoric viscous stress tensor. The single temperature energy equation ($T_i = T_e = T$) is given by

$$\frac{\partial e}{\partial t} = -\frac{p}{\rho} \nabla \cdot u + \frac{\tau}{\rho} \nabla \cdot u - \nabla \cdot (k \nabla T) - 4 \sigma T^4 \chi_{Planck} + \frac{\eta}{\rho} j^2 \quad (12)$$

where k is the thermal conductivity, σ is the Stefan-Boltzmann constant, T is temperature, and χ_{Planck} is the single group Planck emission opacity. Alternatively, if the optical thickness $1/(\rho \chi_{Planck})$ is of the same order or smaller than the particle scale h , then radiation can be modeled as a diffusion process by adding an additional term to the overall thermal conductivity[24]

$$k_{total} = k + k_{Ross} = k + \frac{4acT_e^3}{3\rho\chi_{Ross}} \quad (13)$$

where $a = 4\sigma/c$ is the radiation density constant. If the temperature is split between ions and electrons, then the two temperature energy equations are given by

$$\frac{\partial e_i}{\partial t} = -\frac{p_i}{\rho} \nabla \cdot u + \frac{\tau}{\rho} \nabla \cdot u - \nabla \cdot (k_i \nabla T_i) + Q_{ei} \quad (14)$$

and

$$\frac{\partial e_e}{\partial t} = -\frac{p_e}{\rho} \nabla \cdot u - \nabla \cdot (k_e \nabla T) - 4 \sigma T_e^4 \chi_{Planck} - Q_{ei} + \frac{\eta}{\rho} j^2 \quad (15)$$

where

$$Q_{ei} = \frac{3m_e Zk}{m_i^2} \frac{(T_e - T_i)}{\tau_e} \quad (16)$$

and the electron collision time is[25]

$$\tau_e = \frac{3}{4\sqrt{2\pi}} \frac{m_i \sqrt{m_e}}{Z\rho} \frac{(kT_e)^{3/2}}{\lambda} \frac{(4\pi\epsilon_0)^2}{q^4} \quad (17)$$

D Electromagnetic Field and Circuit Solver

The propagation of electromagnetic waves, current flow, and electromagnetic forces are determined by solving 1) a coupled set of transmission line equations through the conductors connected self consistently to external circuits and 2) Maxwell's equations via the electric scalar and magnetic vector potential equations, given, respectively, by

$$\frac{\partial \phi}{\partial t} = c^2 \left(\nabla^2 \phi + \frac{\rho_c}{\epsilon_0} \right) \quad (18)$$

and

$$\frac{\partial \mathbf{A}}{\partial t} = c^2 \left(\nabla^2 \mathbf{A} + \mu_0 \mathbf{j} \right) \quad (19)$$

where ϕ is the electric scalar potential, c is the speed of light in a vacuum, ϵ_0 is the permittivity of free space, \mathbf{A} is the magnetic vector potential, μ_0 is the permeability of free space, and \mathbf{j} is the

current density vector. Electric field is computed from ϕ and \mathbf{A} with

$$\mathbf{E} = -\nabla \phi - \frac{\partial \mathbf{A}}{\partial t} \quad (20)$$

and magnetic field is calculated with

$$\mathbf{B} = \nabla \times \mathbf{A} \quad (21)$$

Evaluating \mathbf{B} in this way ensures that $\nabla \cdot \mathbf{B} = 0$ is enforced exactly. The scalar and vector potentials are solved on a background of scattered points (the points do not have to be structured) in which the magnetic field and vector potential points are centered in between the points on which the scalar electric potential and electric field are computed, such as shown in Fig. 2. This is a technique borrowed from the FDTD method in which the grid is staggered to avoid nonphysical oscillations which could be induced by the numerical method if \mathbf{E} and \mathbf{B} are solved at the same physical locations[21].

The potential and current are solved self-consistently between an external circuit model a network of transmission line equations. To explain how the model works, we reference Fig. 3 below. The green circuit represents an example of an external circuit which drives current, voltage, electric, and magnetic fields inside the computational domain. The computational domain is represented by the red, gray, and black physical sph particle and the cyan (electric) and yellow (magnetic) field particles, where the electric and magnetic field points are staggered as shown in Fig. 3.

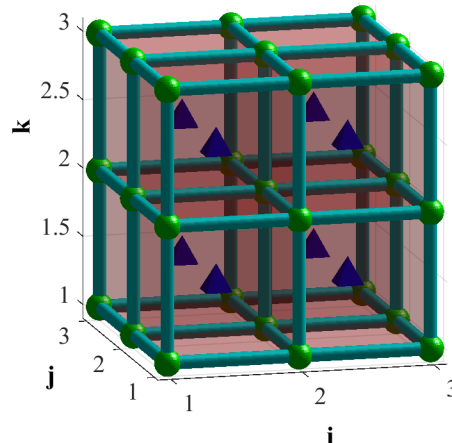


Figure 2. Representative nodes of electric (green circle) and magnetic (blue tetrahedra)

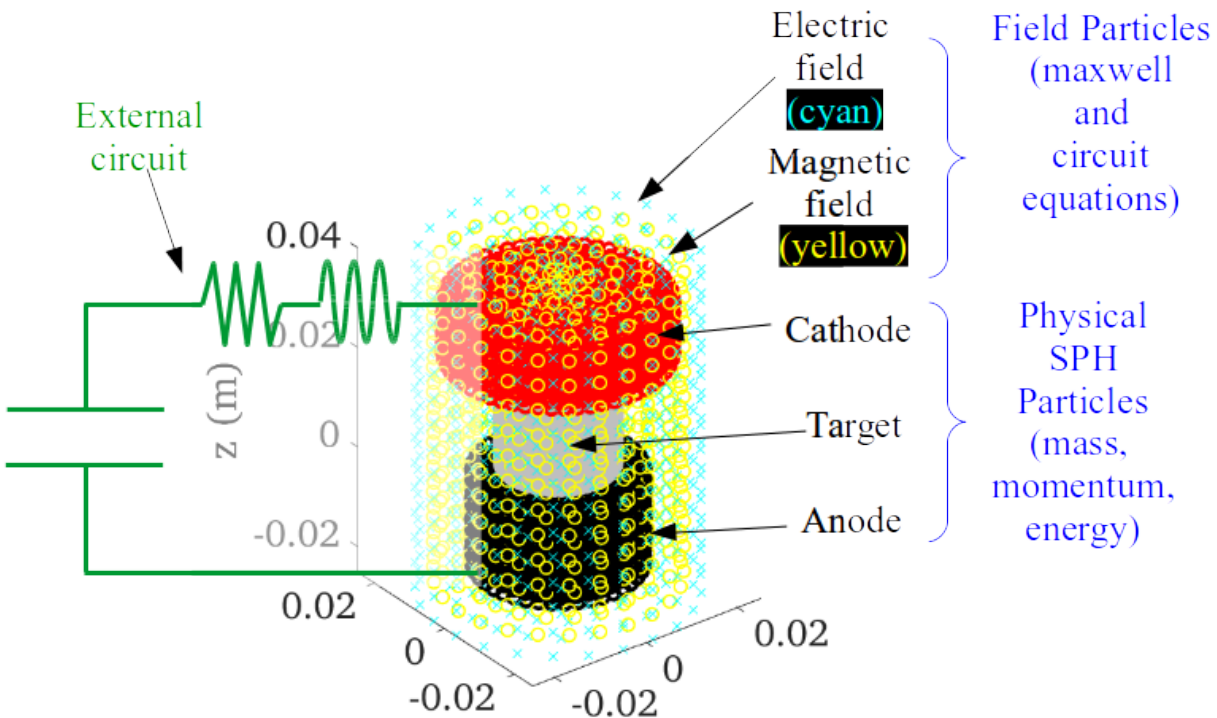


Figure 3. Example of external circuit and connections to anode and cathod of a z-pinch, with SPH particles (red, gray, and black) immersed in electric particles (cyan) and magnetic particles (yellow).

For an external circuit which can be modeled as a series of transmission line sections (including simple RLC circuits, marx banks, pulse forming networks, and linear transformer drivers), the equations are

$$\begin{aligned}
 \dot{V}_1 &= -\frac{I_1}{C_1} \\
 \dot{I}_1 &= \frac{1}{L_1} (V_1 - R_1 I_1 - V_{T,1}) \\
 \dot{V}_{T,1} &= \frac{l_T}{C_T} \left(\frac{I_1 - I_{T,1}}{\Delta z} \right) \\
 \dot{V}_{T,i} &= \frac{l_T}{C_T} \left(\frac{I_{T,i-1} - I_{T,i}}{\Delta z} \right) \quad i = 2 \text{ to } N \\
 \dot{I}_{T,i} &= \frac{l_{T,i}}{L_{T,i}} \left(\frac{V_{T,i} - V_{T,i+1}}{\Delta z} \right) - \frac{I_{T,i} R_{T,i}}{L_{T,i}} \quad i = 1 \text{ to } N-1 \\
 \dot{I}_{T,N} &= \frac{1}{L_{SPH}} (\phi_{SPH, pos} - \phi_{SPH, neg}) - \frac{I_{T,N} R_{T,N}}{L_{T,N}}
 \end{aligned} \tag{22}$$

where the subscript T refers to a transmission line section. Note that the nodes N of the transmission line could be capacitors with their own initial charging voltage, or could/ be bus bars or other passive elements transferring the current and voltage from the capacitor bank to the SPH particles. Note that the last equation, for the time rate of change of current, is directly connected to the SPH particles through the potential difference between the positive and negative SPH particles where the circuit is connected, and the potential is taken to be the mean value for each of the positive and negative electrode leads.

For all SPH particles, the transmission line equations for the physical SPH particles are given as

$$\left(\frac{\partial \phi}{\partial t} \right)_a = - \left(\frac{I}{C'} \right)_a \quad (23)$$

where \mathbf{n} is a unit normal for each face of the particle and C' is the capacitive gradient per particle. The current \mathbf{I} in each particle is advanced in the x, y, and z directions with

$$\frac{\partial I_n}{\partial t} = \frac{-\frac{\partial \phi_n}{\partial n} - (\mathbf{v} \times \mathbf{B})_n + \frac{\partial R}{\partial n} I_n}{\frac{\partial L_n}{\partial n}}, \quad n = x, y, z \quad (24)$$

where

$$R_n = \frac{\rho l}{A_n} \quad (25)$$

Current density in each particle is given by

$$j_n = I_n / A_n \quad (26)$$

and charge density with

$$\frac{\partial \rho}{\partial t} = \frac{1}{vol} I \cdot n \quad (27)$$

where the I_n term is the net current into the particle. In order to connect the external circuit to the SPH particles, the current from the external circuit is added to the positive and negative SPH particles where the circuit is connected. This will add potential to those boundary particles at a rate of I/C . Also, these boundary particles are set with a total current rise rate equal to $\dot{I}_{T,N}$ from the external circuit transmission line equations above.

E Ray tracing for electromagnetic radiation deposition, beam current deposition, fast ion deposition from fusion and fission, and fast fission reactions.

Nonlocal deposition of energy from radiation sources is a challenging problem. The philosophy behind SPFMax is to implement algorithms which capture the physics accurately while maintaining the ability to run full 3D problems on a laptop or comparable desktop computer. The ray tracing algorithm implemented here is an attempt to handle nonlocal deposition with the ability to scale up as computers become more powerful. The basic approach is to specify a ray geometry and a type of source radiation (electromagnetic, fast ions from fusion or fission fragments, neutrons, or current), and the power of the radiation attenuates as it propagates through matter. There are exceptions to the attenuation, such as the specification of a current in a

beam, which could be used to define a simple localized arc. Scattering is currently not modeled. The method assumes a single pass of the radiation from the source along the center axis of the ray or branch (see next paragraph for definition of rays and branches). We may explore including scattering in the future if it becomes important for problems of interest.

Collectively, here the term 'ray' means a beam (i.e. cylinder), axisymmetric cone, or 4π isotropic source of radiation in which the radiation/matter interaction occurs, as illustrated in Fig. 3. The intensity of the radiation source falls off as $1/r^2$ away from the source for the cone and 4π rays, but is collimated for the beam source. In any problem, the user is free to specify any number or combination of rays, although increasing the number and resolution of each ray will slow down the computation. The 4π rays are unique among the 3 ray options in that they are split into a number of 'branches' specified by the user so that anisotropic material properties may interact with an isotropic source, so that heating or other interactions away from the source may vary in any direction, down to the resolution of the branches.

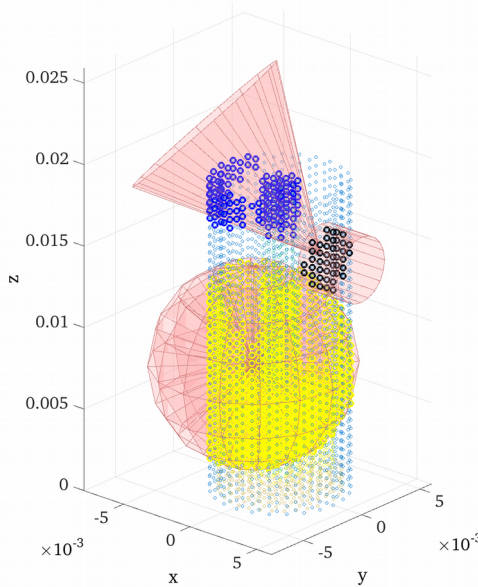


Figure 4. Options for ray tracing, showing a representative beam (cylinder), conical, and 4π (spherical) options. The black, blue, and yellow points are physical SPH particles which reside in each of the beam, cone, and 4π rays, and are the particles which would interact with the radiation source

The present physics options for rays include ohmic dissipation, electromagnetic radiation, and fusion or fission fragment ion deposition. We discuss the models below.

Ohmic dissipation

The energy equation includes a term given by

$$\left(\frac{de}{dt}\right)_{ohmic} = \frac{\eta}{\rho} j^2 \left[\frac{m^2}{s^3} \right] \quad (28)$$

Ohmic Power dropped in a ray segment is given by

$$P_{\Omega,r} = \sum_{b=1}^{N_{p,r}} \frac{\eta_{b,r}}{\rho_{b,r}} j_r^2 \quad (29)$$

where the subscript b,r means particle b in ray segment r, r means ray segment r, and $N_{p,r}$ is the number of particles in ray segment. Note the current is still set up with the circuit. Setting up a ray in this way limits the current to only dissipate energy inside the beam and nowhere else.

Bremsstrahlung radiation power per unit mass

For electromagnetic radiation, if the Bremsstrahlung option is turned on, then the radiation power added to the energy equation is[3]

$$\begin{aligned} \left(\frac{de}{dt}\right)_{br} &= \frac{-16\pi}{3\sqrt{6}\pi} \frac{q^6}{m_e^2 c^3 (4\pi\epsilon_0)^3} \frac{Z_i^2 n_e}{\sqrt{k_B T_e / m_e} MW_i m_a} \int_0^\infty 4\pi \exp \frac{-hv}{k_B T_e} dv \\ &= \frac{-64\pi^2}{3\sqrt{6}\pi} \frac{q^6}{m_e^2 c^3 (4\pi\epsilon_0)^3} \sqrt{\frac{k_B T_e}{m_e}} \frac{Z_i^3 \rho}{(MW_i m_a)^2} \end{aligned} \quad (30)$$

For spectrally dependent (i.e. multigroup) Bremsstrahlung radiation,

$$\left(\frac{de}{dt}\right)_{br_v} = \frac{-64\pi^2}{3\sqrt{6}\pi} \frac{q^6}{m_e^2 c^3 (4\pi\epsilon_0)^3} \sqrt{\frac{k_B T_e}{m_e}} \frac{Z_i^3 \rho}{(MW_i m_a)^2} \left(e^{-\frac{hv_{i+1}}{k_B T_e}} - e^{-\frac{hv_i}{k_B T_e}} \right) \quad (31)$$

The Bremsstrahlung absorption coefficient (free free opacity), and works exactly like the mass attenuation coefficient

$$\kappa_v = \frac{8\pi}{3\sqrt{6}\pi} \frac{q^6}{h m_e^2 c (4\pi\epsilon_0)^3} \frac{Z_i^3 \rho}{(MW_i m_a)^2 v^3} \sqrt{\frac{m_e}{k_B T_e}} = \frac{\mu}{\rho} \left[\frac{m^2}{kg} \right] \quad (32)$$

As a side note, the NIST mass attenuation tables give a parameter (μ/ρ) which is the same thing as κ_v and can be used for the attenuation through solid materials. Finally, the Bremsstrahlung power dropped in a ray segment is given by

$$P_{v,r} = P_{in,v,r} \left(1 - e^{-\kappa_v \rho \Delta r} \right) \quad (33)$$

where the power distributed in each ray segment is given by

$$P_{v,0r} = \left(\frac{de}{dt} \right)_{br_v} \frac{\Omega_r}{4\pi} \quad (34)$$

and the solid angle subtended by the ray is

$$\Omega_r = \sin \phi d\phi d\theta \quad (35)$$

where ϕ is the angle from the z-axis (polar angle) and θ is the azimuthal angle measured CCW from the x-axis around the z-axis.

Fusion power

The reactivity for a reaction of species i with species j is given by

$$\frac{dN}{dt} = \frac{n_{X_i} n_{X_j}}{1 + \delta_{ij}} \langle \sigma v \rangle_{ij} \mathcal{V} \quad (36)$$

where $\delta_{ij} = \begin{cases} 1 & i=j \\ 0 & i \neq j \end{cases}$. The power per unit mass delivered to a particular fusion product specie k is

$$\left(\frac{de}{dt} \right)_k = \frac{n_{X_i} n_{X_j}}{\rho (1 + \delta_{ij})} \langle \sigma v \rangle_{ij} E_k \quad (37)$$

where E_k is the initial kinetic energy of the fusion product specie k. The total power of the system is

$$P_{fus,k} = \sum_{a=1}^N \frac{n_{a,X_i} n_{a,X_j}}{(1 + \delta_{ij})} \langle \sigma v \rangle_{a,ij} E_k \mathcal{V}_a \quad (38)$$

where the sum is over all SPH particles. The fusion power dropped in ray segment is then calculated, starting with the fraction of power in a particular ray with

$$f_r = \frac{\Omega_r}{4\pi} \quad (39)$$

The work done by a fast fusion ion traveling through a particular segment i of a particular ray r is

$$\delta W_{ir} = \left(\frac{dE}{dr} \right)_{ir} \Delta r_{ir} \quad (40)$$

where $(dE/dr)_{ir}$ is the function giving the local stopping power (deceleration force) on the fast particles determined as a function of ion species and electron densities and temperatures. The local stopping power itself is a function of the kinetic energy of the fast ions moving through the ray segment, $0.5 m_k v_{k,ir}^2$. It is assumed that through a ray segment, the stopping power is constant. The total change of kinetic energy of the ion in the segment is then

$$\frac{1}{2} m_k v_{k,ir}^2 - \frac{1}{2} m_k v_{k,i(r-1)}^2 = -\delta W_{ir} \quad (41)$$

The velocity is then

$$v_{k,ir} = \max \left[\left(v_{k,i(r-1)}^2 - \frac{2\delta W_{ir}}{m_k} \right), 0 \right] \quad (42)$$

The ion deposition power dropped in a ray segment is finally

$$P_{ion,0r} = \left(\frac{n_{X_i} n_{X_j}}{1 + \delta_{ij}} \langle \sigma v \rangle_{ij} \mathcal{V} \right) \left(\frac{\Omega_r}{4\pi} \right) \left(\left(\frac{dE}{dr} \right)_{ir} \Delta r_{ir} \right) \quad (43)$$

The stopping power models are not discussed here, but examples in the literature include Harris and Miley[26], Long and Tahir[27], and most recently by Grabowski et al[28].

Fission power

The fission power is determined assuming a single pass of fast neutrons from a fusion source, fission source, or user-specified source, and is given for a ray segment i of a particular ray r as

$$P_{fis} = \left(\frac{dN}{dt} \right)_{neutrons} f_r n_{ir} \sigma_{fis} \Delta r_{ir} Q_{fis} \quad (1)$$

where n_{ir} is number density of the fission fuel reacting with the neutrons, σ_{fis} , is the fast fission cross section which needs to be a function of the energy of the neutron from the fusion reactions and the species it is reacting with, and Q_{fis} is the energy released per reaction. This model is specifically in support of modeling of the advanced fission fusion propulsion concept ‘Puff’[29].

III. Initial conditions for a spherical plasma liner imploding on a magnetized target

This section should be prefaced by the fact that while many aspects of the hydrodynamics and plasma dynamics of SPFMax have been verified including shock capturing, thermal conduction, and radiation emission[30]–[32], we are only beginning to test the electromagnetic and radiation/matter matter interactions. The results presented in this paper are not rigorously verified, but do inform us of challenges we face in using the methods, while comparisons of our results with other models provide insight into the usefulness of the methods given here.

For the 3D simulation presented in this paper, we chose a representative high gain case from Knapp and Kirkpatrick[22]. An Argon liner of thickness 6.6 cm and initial radius of 4.7 cm with density of 36 kg/m^3 and initial implosion velocity of 60 km/s impinges on a stationary DT target of density 0.018 kg/m^3 and 80 eV. In the 1D simulations of Knapp and Kirkpatrick the magnetic field is just specified as orthogonal to the radial implosion. In the present case, we chose a so-called force free magnetic topology which is a solution to

$$\nabla \times \mathbf{B} = \lambda \mathbf{B} \quad (44)$$

Here, ‘force free’ means that \mathbf{j} and \mathbf{B} are every parallel and λ is an eigenvalue and is spatially constant. This configuration was chosen because it has been shown that a simply connected, enclosed field topology with a conductive boundary will relax through MHD instabilities to this state[33], [34]. The solution for a spherically enclosed system gives the radial magnetic field as,

$$B_r = \frac{2 B_0 \cos(\theta) j_1(kr)}{kr} \quad (45)$$

The azimuthal field is given with

$$B_\phi = B_0 \sin(\theta) j_1(k r) \quad (46)$$

and the polar field is given with

$$B_0 = \frac{-B_0 \sin(\theta)}{k r} \frac{d}{dr} [r j_1(k r)] \quad (47)$$

where j_1 is the spherical Bessel function and $k r_s = 4.49$. For reference, the spherical Bessel function is

$$j_1(x) = J_{1+1/2}(x) \sqrt{\frac{\pi}{2x}} \quad (48)$$

where J is the ordinary Bessel function. The current density for these functions is given by

$$\mathbf{j} = \frac{k \mathbf{B}}{\mu_0} \quad (49)$$

and the vector potential is given by

$$\mathbf{A} = \frac{\mathbf{B}}{k} \quad (50)$$

For the simulations, we chose the flux radius as 4.2 cm and set $B_0=1$ T. While 3D enclosed magnetic field topologies may be difficult to visualize, we make an attempt below with the stream ribbon plot, Fig. 5a, and contour slice plots through the $x=0$ and $z=0$ planes, Fig. 5b. In both plots, the color is scaled against the magnitude of the magnetic field in units of Tesla.

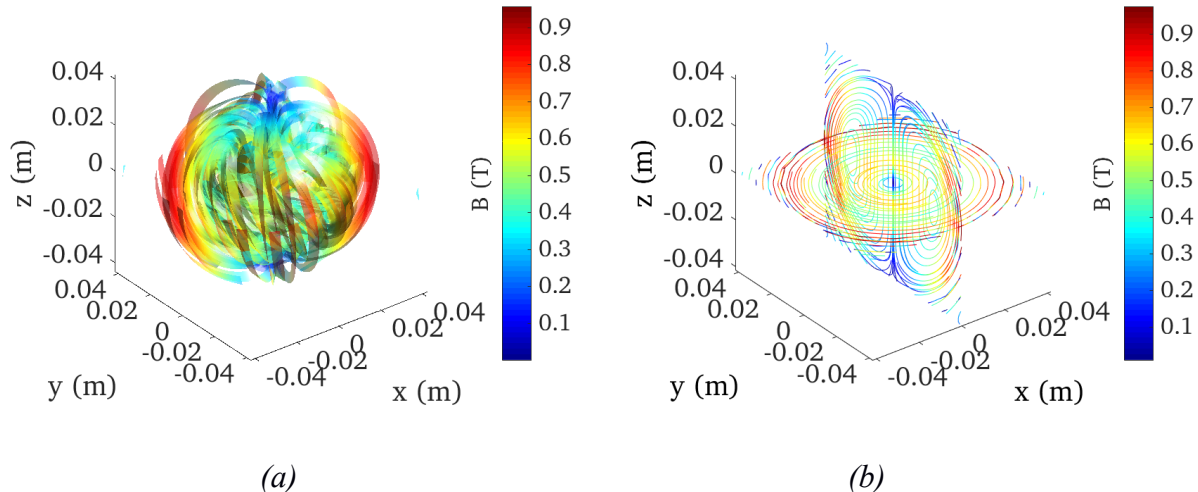


Figure 5. Initial magnetic field in a spherical spheromak illustrated by a) stream ribbon plot and b) streamslice plots showing poloidal and toroidal field components. Stream color is scaled against magnetic field strength in Tesla.

IV. Results

The model was run until 600 ns, at which point the simulation crashed. However, quite a bit of information could be extracted from the output during that time. Mass density slices at 0, 250,

500, and 600 ns show that the liner compresses the target and remains mostly spherical, with target density increase by a factor of 100, Fig. 6. The ion temperature of the deuterium tritium target increases from 80 to 1000 eV, during this time, Fig. 7. Early in the simulation, the magnetic field appears to rotate, and quickly diffuses to the outer surface of the liner, Fig. 8. The strength of the field in the target remains more or less constant, around 1 T. Rayleigh-Taylor instabilities begin to develop, creating perturbations on the surface of the target which is visible in all of the plots at 600 ns. In the near future we will resolve the numerical problem which caused the simulation to crash, and extend the run until the fusion reactivity drops to negligible values. Figure 9 gives the fusion charged particle energy and neutron yield vs time up until the model ends, showing a steady increase in fusion power.

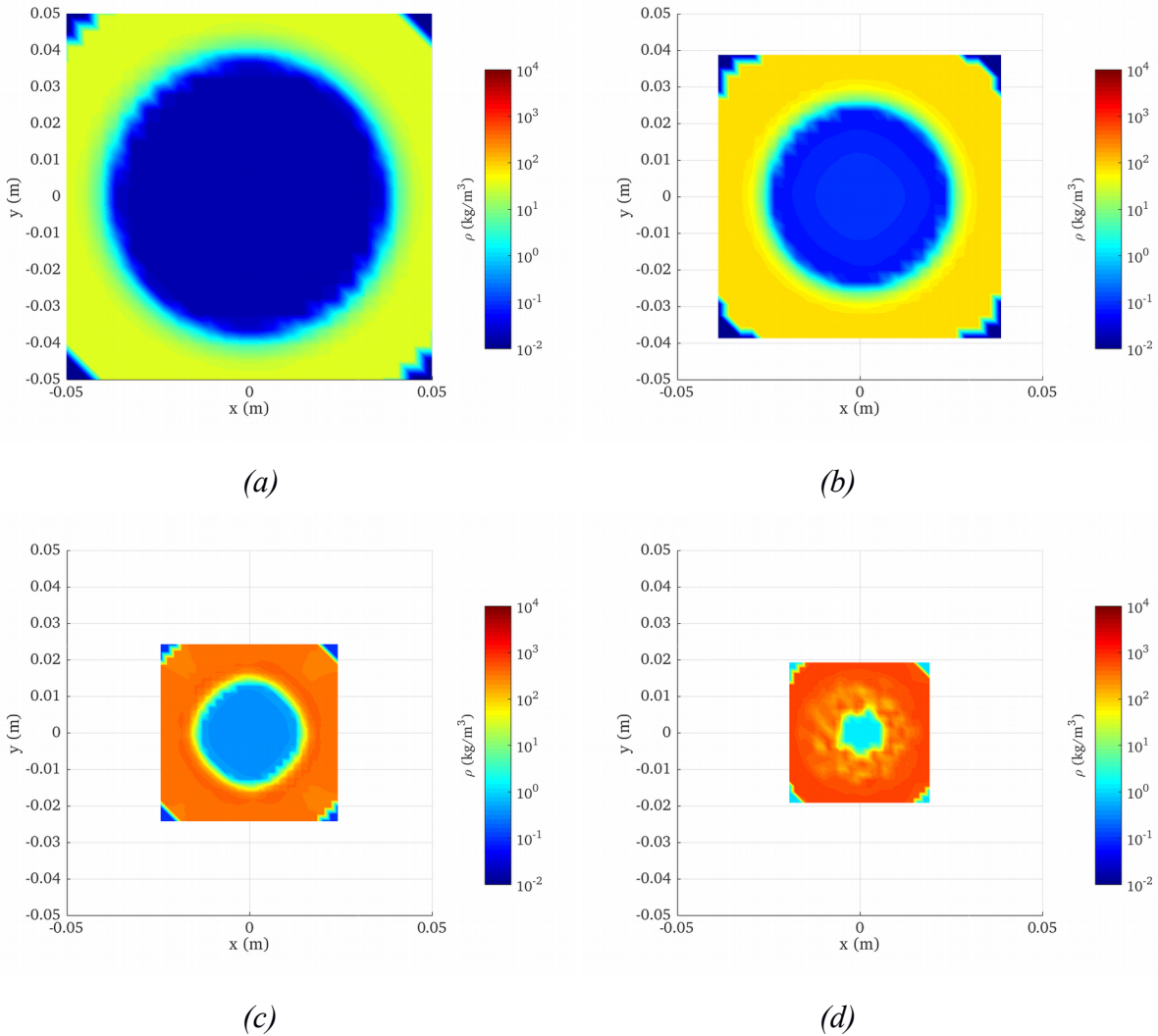


Figure 6. $z=0$ slice of mass density for a) 0 ns, b) 250 ns, c) 500 ns, and d) 600 ns..

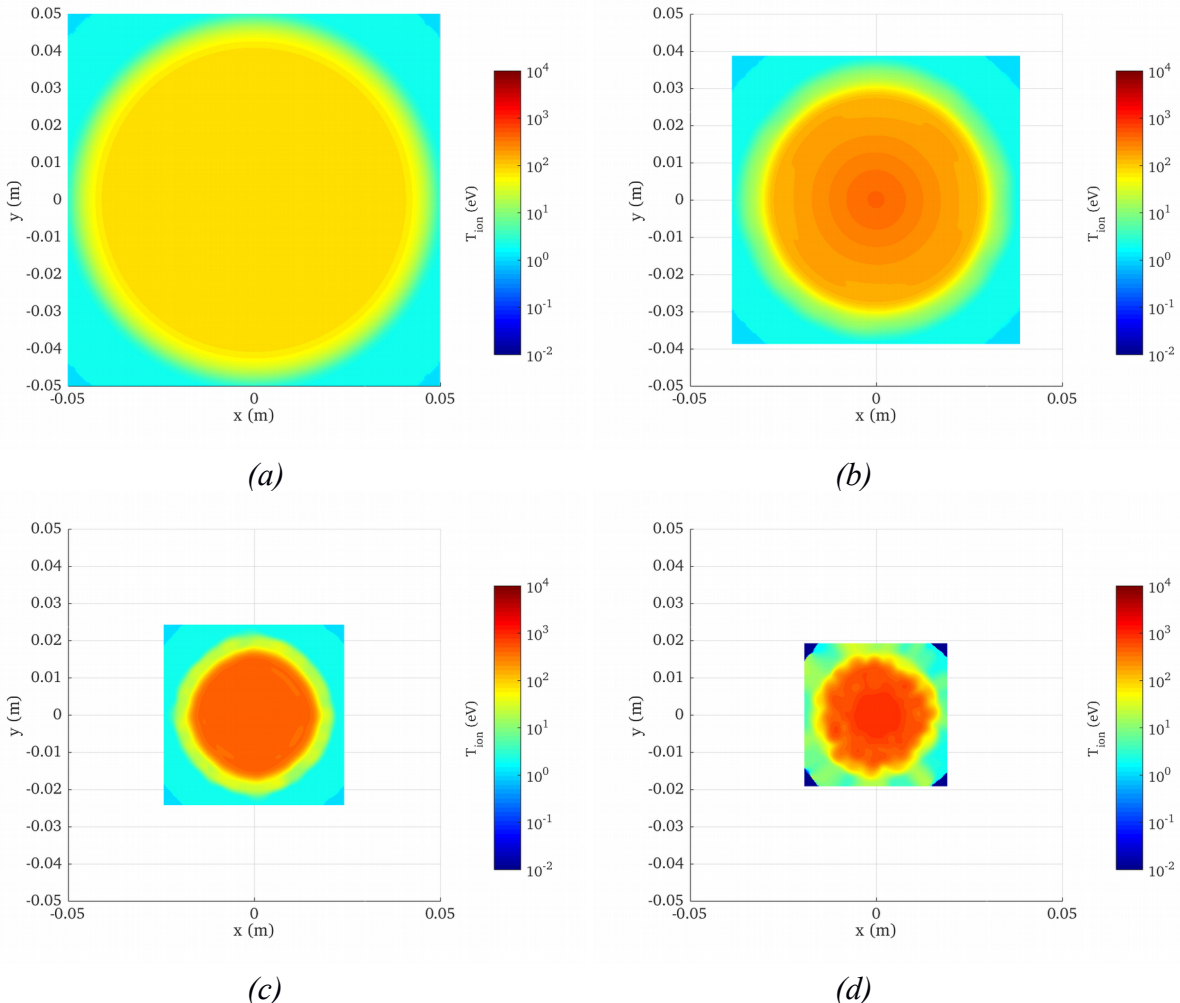


Figure 7. $z=0$ slice of temperature for a) 0 ns, b) 250 ns, c) 500 ns, and d) 600 ns.

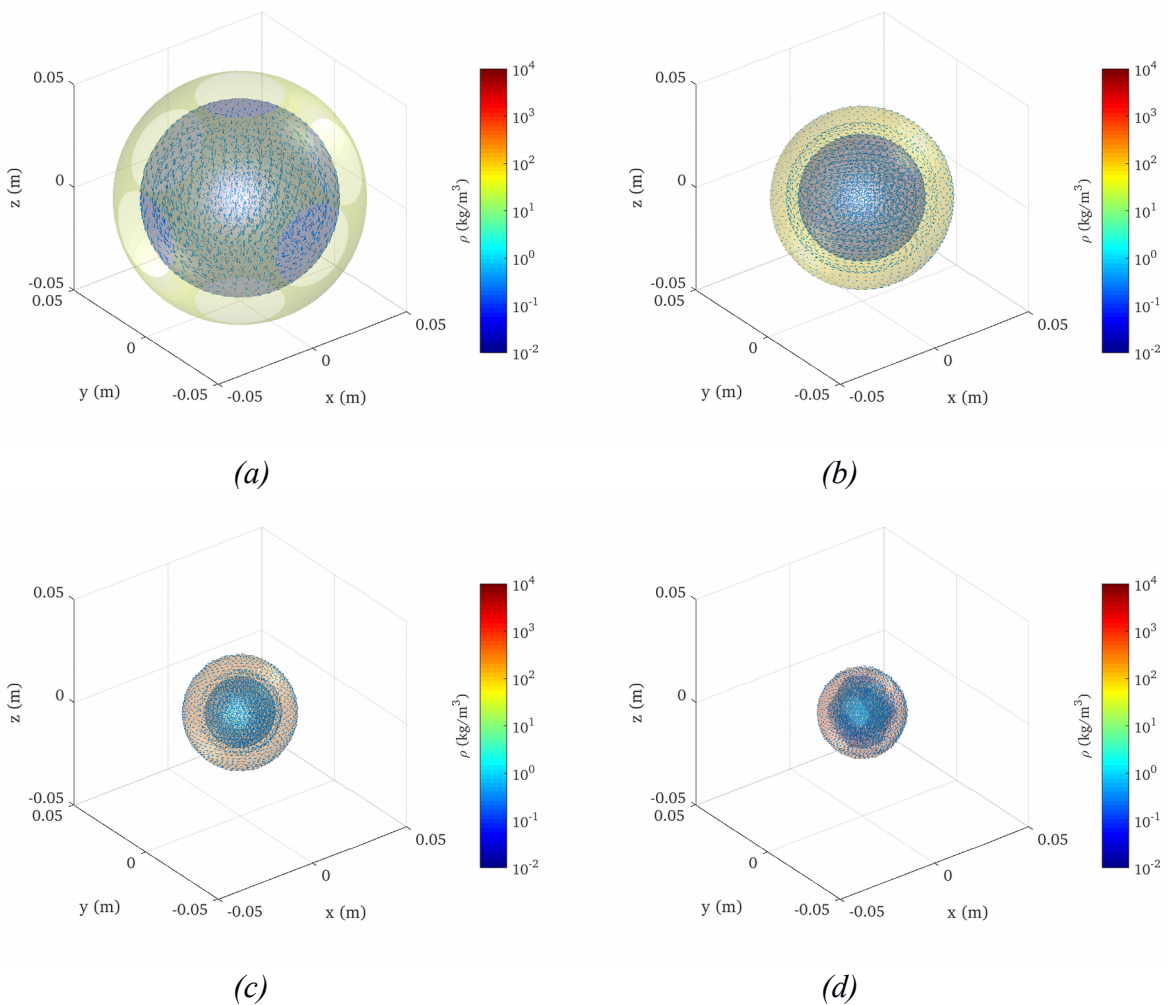


Figure 8. Outer surface plots of liner and target with color scaled to mass density, with vector plot of magnetic field components at a) 0 ns, b) 250 ns, c) 500 ns, and d) 600 ns.

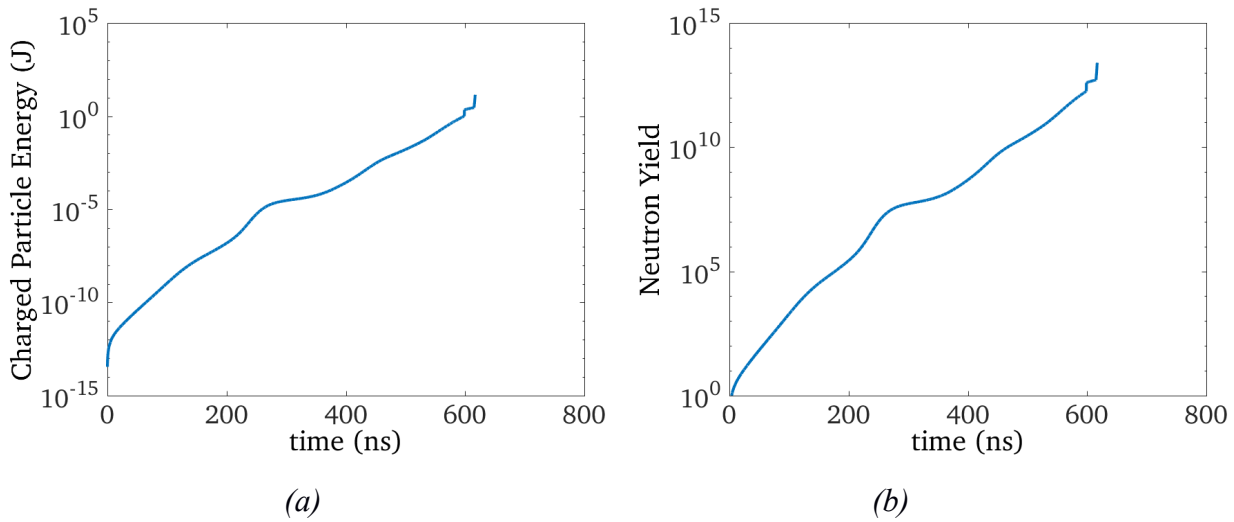


Figure 9. Time history of a) fusion charged particle energy and b) neutron yield.

V. Conclusions

A 3D Smooth Particle with Maxwell equation solver (SPFMax) code has been developed in Matlab to perform magneto-inertial fusion simulations capable of being performed on a standard desktop. The fluid is modeled using smooth particle hydrodynamics, and is coupled to an external circuit model and internal transmission line model which advances the current and potential using a 3D network of Kirchoff's voltage and circuit laws. The electric and magnetic fields are advanced using the electric scalar potential and magnetic vector potential. Fusion reaction rates are included, along with nonlocal deposition of fusion charged particles and multigroup radiation via a relatively simple ray tracing algorithm. A preliminary simulation of a plasma liner compressing a magnetized target has been performed, with the outer 60 km/s Argon liner compressing a 50/50 mixture of deuterium and tritium. Although the model crashed at 600 ns in this trial run, the target was compressed 100 times its initial density and increased in temperature from 80 to 1000 eV. The magnetic topology was initially a spheromak and appeared to rotate early in the simulation, while retaining a closed field topology during most of the run. The field partially diffused into the surrounding liner, retaining roughly the same magnetic field strength of 1 T in the target. Fusion energy and neutron yield were seen to steadily rise during the simulation. Reasons for the simulation halting are under investigation, but the basic methods in SPFMax appear to be promising for being able to study magneto-inertial fusion.

Acknowledgments

This work was supported in part by ARPA-E DOE Award Number DE-AR0000566, Pulsed Fission-Fusion Propulsion NASA Contract NNM11AA01A, and NASA Innovative Advanced Concepts.

References

- [1] I. R. Lindemuth and R. E. Siemon, "The fundamental parameter space of controlled thermonuclear fusion," *Am. J. Phys.*, vol. 77, no. 5, pp. 407–416, 2009.
- [2] J. Cassibry *et al.*, "Case and Development Path for Fusion Propulsion," *J. Spacecr. Rockets*, vol. 52, no. 2, pp. 595–612, 2015.
- [3] S. Atzeni and J. Meyer-ter-vehn, *The Physics of Inertial Fusion*. Oxford: Clarendon Press, 2004.
- [4] R. Lovberg and S. Glasstone, *Controlled thermonuclear reactions, an introduction to theory and experiment*. CONTROLLED THERMONUCLEAR REACTIONS, AN INTRODUCTION TO THEORY AND EXPERIMENT, BY SAMUEL GLASSTONE AND RALPH H. LOVBERG. PRINCETON, N. J., VAN NOSTRAND (1960), 1960.
- [5] R. J. Goldston and P. H. Rutherford, *Introduction to Plasma Physics*. Bristol and Philadelphia: Institute of Physics Publishing, 1997.
- [6] W. W. Gibbs, "The Fusion Underground," *Sci. Am.*, vol. 315, no. 5, pp. 38–45, Nov. 2016.

- [7] R. B. Adams *et al.*, “Conceptual Design of In-Space Vehicles for Human Exploration of the Outer Planets,” NASA/TP-2003-212691, Nov. 2003.
- [8] Y. C. F. Thio, C. E. Knapp, R. C. Kirkpatrick, R. E. Siemon, and P. J. Turchi, “A Physics Exploratory Experiment on Plasma Liner Formation,” *J Fusion Energy*, vol. 20, no. 1/2, pp. 1–11, 2001.
- [9] R. P. Drake, J. H. Hammer, C. W. Hartman, L. J. Perkins, and D. D. Ryutov, “Submegajoule Liner Implosion of a Closed Field Line Configuration,” *Fusion Technol.*, vol. 30, no. 3, pp. 310–325, 1996.
- [10] M. M. Marinak *et al.*, “Three-dimensional HYDRA simulations of National Ignition Facility targets,” *Phys. Plasmas*, vol. 8, p. 2275, 2001.
- [11] R. E. J. Peterkin, M. H. Frese, and C. R. Sovinec, “Transport of Magnetic Flux in an Arbitrary Coordinate ALE Code,” *J. Comput. Phys.*, vol. 140, pp. 148–171, 1998.
- [12] G. B. Zimmerman and W. L. Kruer, in *Comments on Plasma Physics and Controlled Fusion*, vol. 2, 1975, p. 51.
- [13] D. R. Welch, D. V. Rose, B. V. Oliver, and R. E. Clark, “Simulation techniques for heavy ion fusion chamber transport,” *Nucl. Instrum. Methods Phys. Res. Sect. Accel. Spectrometers Detect. Assoc. Equip.*, vol. 464, no. 1–3, pp. 134–139, May 2001.
- [14] J. Cassibry *et al.*, “The Case and Development Path for Fusion Propulsion,” 2012.
- [15] J. Cassibry *et al.*, “The Tendency of Plasma Liners Formed by Hypersonic Jets to Evolve Toward Good Spherical Symmetry During Implosion,” *Bull. Am. Phys. Soc.*, vol. Volume 56, Number 16, Nov. 2011.
- [16] R. A. Agnew, J. T. Cassibry, and B. H. Winterling, “Analytic Model to Estimate Thermonuclear Neutron Yield in Z-Pinches Using the Magnetic Noh Problem,” *IEEE Trans. Plasma Sci.*, vol. 44, no. 10, pp. 2181–2189, Oct. 2016.
- [17] J. P. Freidberg, “Ideal Magnetohydrodynamic theory of magnetic fusion systems,” *Rev. Mod. Phys.*, vol. 54, no. 3, pp. 801–902, 1982.
- [18] D. J. Price, “Smoothed Particle Hydrodynamics and Magnetohydrodynamics,” arXiv e-print 1012.1885, Dec. 2010.
- [19] G. Tóth, “The $\text{div} \cdot \mathbf{B} = 0$ Constraint in Shock-Capturing Magnetohydrodynamics Codes,” *J. Comput. Phys.*, vol. 161, pp. 605–652, 2000.
- [20] C.-D. Munz, P. Omnes, R. Schneider, Sonnendrücker, and U. Voß, “Divergence Correction Techniques for Maxwell Solvers Based on a Hyperbolic Model,” *J. Comput. Phys.*, vol. 161, pp. 484–511, 2000.
- [21] A. Elsherbeni and V. Demir, *The Finite Difference Time Domain Method for Electromagnetics: With MATLAB Simulations*, Har/Cdr. SciTech Publishing, 2009.
- [22] C. E. Knapp and R. C. Kirkpatrick, “Possible energy gain for a plasma-liner-driven magneto-inertial fusion concept,” *Phys. Plasmas*, vol. 21, no. 7, p. 070701, Jul. 2014.
- [23] J. J. Monaghan, “Smoothed Particle Hydrodynamics,” *Rep. Prog. Phys.*, p. 57, 2005.
- [24] Y. B. Zel'dovich and Y. P. Raizer, *Physics of Shock Waves and High-Temperature Hydrodynamic Phenomena*. Meneola, New York: Dover Publications, Inc., 2000.

- [25] J. D. Huba, “NRL: Plasma Formulary,” NAVAL RESEARCH LAB WASHINGTON DC BEAM PHYSICS BRANCH, NAVAL RESEARCH LAB WASHINGTON DC BEAM PHYSICS BRANCH, NRL/PU/6790--04-477, Dec. 2004.
- [26] D. B. Harris and G. H. Miley, “Burn performance of inertial confinement fusion targets,” *Nucl. Fusion*, vol. 28, no. 1, p. 25, 1988.
- [27] K. A. Long and N. A. Tahir, “Theory and calculation of the energy loss of charged particles in inertial confinement fusion burning plasmas,” *Nucl. Fusion*, vol. 26, no. 5, p. 555, 1986.
- [28] P. E. Grabowski, M. P. Surh, D. F. Richards, F. R. Graziani, and M. S. Murillo, “Molecular Dynamics Simulations of Classical Stopping Power,” *Phys. Rev. Lett.*, vol. 111, no. 21, p. 215002, Nov. 2013.
- [29] R. B. Adams, J. T. Cassibry, and K. Schillo, “Developing the Pulsed Fission-Fusion (PuFF) Engine,” in *50th AIAA/ASME/SAE/ASEE Joint Propulsion Conference*, American Institute of Aeronautics and Astronautics.
- [30] J. C. Cassibry, R. Samulyak, K. Schillo, W. Shih, and S. C. Hsu, “Numerical Modeling of Plasma-Liner Formation and Implosion for the PLX-{\$}\backslash alpha{\$} Project,” in *Bulletin of the American Physical Society*, San Jose, CA, 2016, vol. 61 (18).
- [31] J. Cassibry, S. Hsu, K. Schillo, R. Samulyak, P. Stoltz, and K. Beckwith, “Modeling of the merging, liner formation, implosion of hypervelocity plasma jets for the PLX-\$\alpha\$ project,” in *Bulletin of the American Physical Society*, 2015, vol. Volume 60, Number 19.
- [32] K. Schillo, J. Cassibry, and S. Hsu, “Effects of real viscosity on plasma liner formation and implosion from supersonic plasma jets,” in *Bulletin of the American Physical Society*, 2015, vol. Volume 60, Number 19.
- [33] J. B. Taylor, “Relaxation of Toroidal Plasma and Generation of Reverse Magnetic Fields,” *Phys. Rev. Lett.*, vol. 33, no. 19, pp. 1139–1141, Nov. 1974.
- [34] P. M. Bellan, “Generalization of cylindrical spheromak solution to finite beta and large reversed shear,” *Phys. Plasmas*, vol. 9, no. 7, pp. 3050–3056, Jun. 2002.